Edelweiss Applied Science and Technology
ISSN: 2576-8484
Vol. 8, No. 6, 7404-7418
2024
Publisher: Learning Gate
DOI: 10.55214/25768484.v8i6.3604

Dynamic characteristics of micro-perforated complex beam structures

Vu Van The[1*]
[1]Faculty of Mechanical Engineering, Le Quy Don Technical University, Hanoi, 100000, Vietnam; vuvanthe@lqdtu.vn (V.V.T.).

Abstract: This paper discusses research concerning the fluctuating dynamic characteristics of various micro-beams featuring intricate designs and perforated surfaces across their entire operational faces. The complex beam structures consist of different types: folded beam, V-shaped beam, and crab-shaped beam with different boundary conditions: fixed-free, fixed-fixed for the simple single beam, and fixed-guided for the rest. The types of holes on the body of the beams are choice in square and circle-shaped for common. In addition, the methodology to determine the dynamic characteristics of the perforated beam is also proposed based on using FEM simulation software. The results show that the dynamic characteristics of the beam in which the holes are distributed depend on the size and shape of perforated holes. As the size or quantity of holes on the surface of the beam in perforated micro-beams grows, the equivalent stiffness drops noticeably. Consequently, the fundamental frequencies of the MEMS systems that include these micro-beams also diminish. The damping coefficient also reduces thanks to the occurrence of these holes. The maximum decrease in damping coefficient reaches 84% in the ideal case for the crab-shaped beam with square holes. These results can be used to optimize the MEMS structures in future research.

Keywords: *Dynamic characteristics, MEMS devices, Micro-beam, Perforated beam.*

1. Introduction

Microtechnology is a field of technology that encompasses features with measurements of one micrometer [1]. It concentrates on the production or manipulation of structures with a one-micrometer magnitude, as well as chemical and physical procedures [2]. MEMS has been recognized as a very promising technology for the 21st century, with the ability to transform both industrial and consumer goods via the integration of silicon-based microelectronics and micromachining innovation. Its methodologies and microsystem-based technologies have the potential to significantly impact our lives and lifestyles . Therefore, in the field of computational mechanics, the analysis of mechanical behavior of beam, plate and shell structures plays an important role in the calculation and design of microelectromechanical devices [3], [4].

For beam structures, they are often used in mechanical constructions to facilitate the anticipated motion of the moving component. The mechanical configurations of micro-electro-mechanical systems (MEMS) are essential for performing the fundamental operations of microactuators or microsensors. The beams operate analogously to springs in mechanical vibration systems because of their elastic material qualities. The deformation of these beams in designated design orientations generates the necessary vibrational modes inside the mechanical system. The arrangement of the micro beams may be configured differently based on the intended motion of the mass element in each vibration system. The beams may be configured in several designs, including single beam [5], folded beam [6], [7], multi-folded beam [8], crab-shaped beam [7], T-shaped beam [8], Z-shaped beam, and V-shaped beam [9]. The mechanical reactions of these beam configurations have been analyzed under the premise of a completely filled state with a uniform cross-section. The approach presumes linear elastic material behavior and neglects substantial structural deformations.

The square-shaped perforations along the beams lead to a decrease in the beam's mass, which subsequently reduces the residual stress within the beam [10]. The holes created in the beam and resonator bodies have been identified as an effective method for minimizing the beam's effective mass and

* Correspondence: vuvanthe@lqdtu.vn

mitigating the influence of squeeze film damping. These two elements are pivotal in determining the switching speed in the MEMS switches [11]. To enhance the sensitivity in the MEMS resonators, it is necessary to reduce the effective mass and increase the active area for their beams [12]. Although the cutout holes have a minor impact on pull-in voltage, they result in decreased equivalent stiffness and lower effective elastic modulus of the meander flexure MEMS switch [13].

Perforated apertures are often seen in the manufacturing of MEMS. They are generated during the etching procedure of the sacrificial layer. Perforated MEMS beams have a regular arrangement of apertures or slots throughout their length. The presence of these holes may influence the mechanical properties of the beam, including its stiffness, resonant frequency, and damping characteristics.

The analysis of the single beam is performed using either Euler-Bernoulli or Timoshenko beam theory, based on the assumption that the total stress over the whole cross-section is uniform for both completely filled and equivalent perforated beams. Furthermore, it is anticipated that the stress distribution inside the filled segment of the beam and plates adheres to a linear and continuous pattern [14], [15], [16], [31]-[35]

Despite appearing for merely technological reasons for increasing the etching speed of the sacrificial layer under the beam or plate itself, these perforated holes are demonstrated to affect the mechanical behavior of MEMS structures on various sides [17], [18], [19], [20]. An experimental study on specimens with polysilicon materials has shown that compared with the mechanical characteristics of the specimens without etch holes, the tensile strength has dropped by 50% and Young's modulus decreases only about 18% due to the existence of the etch holes [17], [18]. The plate structures with perforated holes were also studied. The results show that the release hole on the back plate of MEMS devices affects not only the stiffness coefficient but also the damping force of squeeze films in the whole structure [19]. The etching holes often alter the electromechanical properties of the microdevices, especially capacitive devices, because the fringe fields induced by the etching holes can significantly alter the electrical properties [20]. Thai et al. [21], [22] studied the mechanical behavior of micro-sized beam structures taking into account geometrical imperfections. Nhung and coworkers [23] studied the geometric nonlinearity of microplate structures with variable thickness using modified couple stress theory.

This study will identify and present the dynamic characteristics of micro-beams featuring intricate structures with square or circular perforations. The beams analyzed include folded beams, Crab beams, and V-shaped beams, all of which are commonly utilized in MEMS devices. The focus of this research is on dynamic analysis to ascertain the equivalent stiffness and modal analysis to establish the resonant frequencies for various movements influenced by the differently shaped holes within the beams.

The rest of this paper is structured as follows: Section 2 presents the perforated microbeam models. Dynamic characteristics of perforated microbeams are described in Section 3, in which, theories of the perforated single-beam, the equivalent and natural frequencies of perforated micro-beams with complex structures, and air damping with perforated beams are presented in detail. Some of the main results of the paper are presented in section 4.

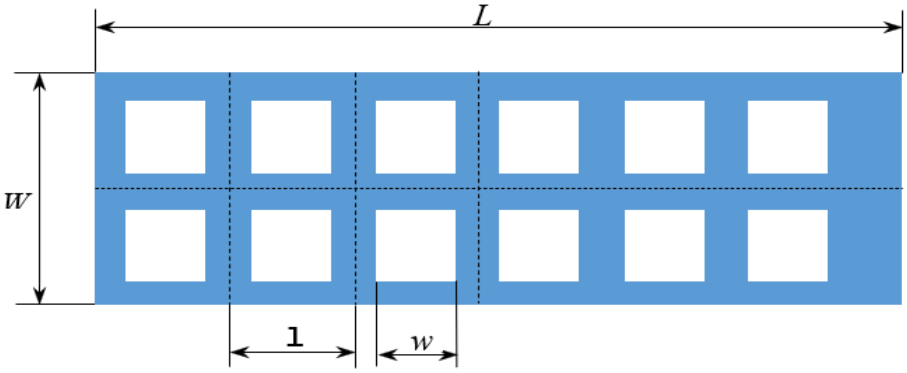

a) Perforated beam with square holes

Edelweiss Applied Science and Technology
ISSN: 2576-8484
Vol. 8, No. 6: 7404-7418, 2024
DOI: 10.55214/25768484.v8i6.3604

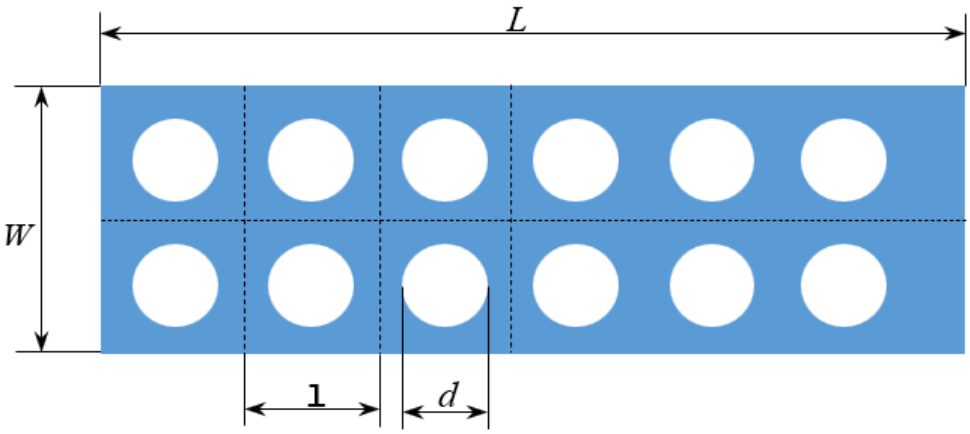

b) Perforated beam with circle holes

Figure 1.
Model of the beam with perforated hole.

2. Perforated Microbeam Models

Some models of Timoshenko or Euler Bernoulli beam with square perforated holes located along the length beam are shown in Figure 1a. These beams are considered with the length L and the cross-section $W \times h$ (where h is the thickness and W is the width of beams). The square hole (edge w) is located at the center of the square meshed grid l. In this study, the square hole w is replated with the circle hole with diameter d ($d = w$) for an additional study case to determine the dynamic characteristics of the perforated Timoshenko beam (Figure 1b).

To evaluate the effect of the perforated holes on the dynamic characteristics of the beams, the fill factor is defined as the proportion of the hole size (either width w or diameter d) to the dimensions of the meshed grid l [12], [24].

$$\alpha = \frac{l-w}{l} = 1 - w/l \text{ or } \alpha = \frac{l-d}{l} = 1 - d/l \quad (1)$$

whereby, the fill factor is considered as $0 \leq \alpha \leq 1$, $\alpha = 0$ represents an unrealistic scenario where the entire beam is cut out ($d = l$ or $w = l$), and $\alpha = 1$ indicates a completely full beam without the holes cutout ($w = d = 0$). As the fill factor decreases, the size of the hole increases. In this study, the values $\alpha = 0$ and $\alpha = 1$ will be excluded to maintain consistency in the models created during the simulation analyses and to suit the research subjects for the paper.

Edelweiss Applied Science and Technology
ISSN: 2576-8484
Vol. 8, No. 6: 7404-7418, 2024
DOI: 10.55214/25768484.v8i6.3604

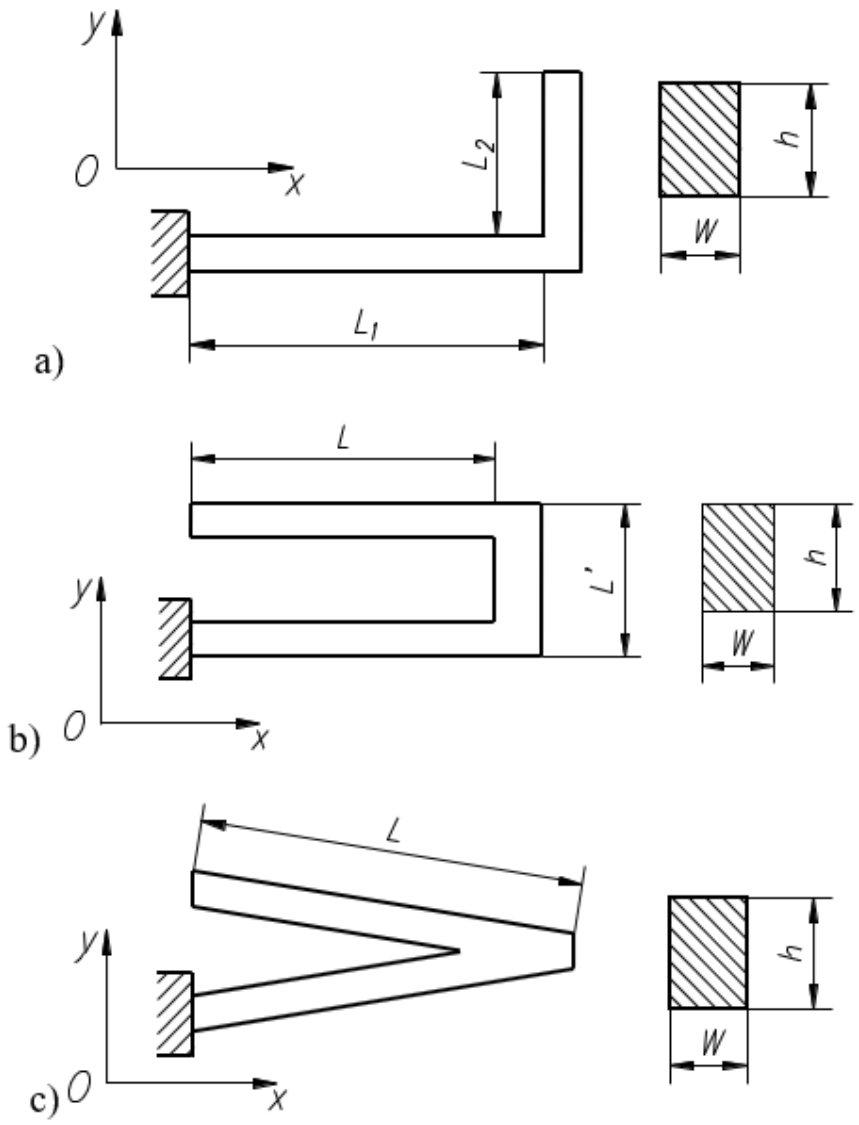

a) Crab-shaped beam, b) Folded beam, and c) V-shaped beam

Figure 2.
The micro-perforated beams with complex structure.

Table 1.
The characteristics of the Silicon material.

Property	Value	Unit
Density	2330	kg/m^3
Poisson's ratio	0.28	1
Young's modulus	169×10^9	Pa
Bulk modulus	1.2803×10^{11}	Pa
Orientation	1-0-0	

To enhance the intricacy of perforated beam designs, the folded beam, the Crab-shaped beam, and the V-shaped beam models are depicted in Figure 2 with the holes arranged uniformly on the working face (parallel to the substrate). These complex beams with solid bodies are frequently utilized in the design of

Edelweiss Applied Science and Technology
ISSN: 2576-8484
Vol. 8, No. 6: 7404-7418, 2024
DOI: 10.55214/25768484.v8i6.3604

mechanical structures in MEMS system. Nevertheless, it is essential to take into account the perforations within their structure and their mechanical behaviors to fully understand the characteristics of the entire system.
Silicon is the standard material utilized for these beams in SOI wafers. The properties of this material can be found in Table 1.

3. Dynamic Characteristics of Perforated Microbeams

3.1. Theories of the Perforated Single Beam

The single beams used in MEMS are known as the Euler-Bernoulli or Timoshenko beam with defined boundary conditions (simply supported, fixed-fixed, simply-fixed, fixed-guided, or fixed-free,…). In the case of the Timoshenko beam, the theory in the analysis of the perforated beam incorporates the effects of shear deformation and axial deformation, along with bending deformation, and was mentioned by considering the interrelated effects of microstructure and surface stress under various loading and boundary conditions [12] when the micro beams were defined with perforated square-shaped holes and using an equivalent geometrical model [25]. As the beam is bent, its cross-section can change shape, leading to the beam being represented as a series of continuous curved segments. This approach enables a more precise representation of both shear and axial deformations, which is particularly crucial for short, thick beams or those that experience significant shear forces.

During the analytical calculation, the resonant frequencies of the Timoshenko beam considered in [24], [26] are defined by using their dynamic equations as follows [25]:

$$EI\frac{\partial^4 u}{\partial x^4}+\rho_A\frac{\partial^2 u}{\partial t^2}-\left(\rho_I+\frac{EI\rho_A}{G_A}\right)\frac{\partial^4 u}{\partial x^2\partial t^2}+\frac{\rho_I\rho_A}{G_A}\frac{\partial^4 u}{\partial x^4}=p(x,t)+\frac{\rho_I}{G_A}\frac{\partial^2 p(x,t)}{\partial t^2} \quad (2)$$

In this context, EI, ρ_A, ρ_I, and G_A denote the bending stiffness, linear density, rotational moment, and shear stiffness of the oscillator, respectively; $u = u(x,t)$ signifies the displacement function of the beam under consideration; and $p(x,t)$ represents the distributed load applied to the beam's surface.

There are many case studies about the boundary constraints of the single beam. The natural frequency of a fixed-fixed single beam is found using the formula [27]:

$$f_n=\frac{1}{2\pi}\sqrt{\frac{EI_{eq}Z^4}{\rho A_{eq}L^4}} \quad (3)$$

Where L is the beam length; E signifies Young's modulus, while ρ denotes the density of the material; EI_{eq} and ρA_{eq} refer to the bending stiffness and the mass per unit length of the perforated beam; and Z is a function that indicates the n^{th} root of the equation dependent on γ, which is treated as a geometry-related variable. The expression describing γ is the following:

$$\gamma=\frac{EI_{eq}}{AG_{eq}L^2} \quad (4)$$

AG_{eq} refers to the shear stiffness of the mentioned beam.

$$AG_{eq}=A\frac{N+1}{N}\frac{E}{2}\alpha^3$$
$$EI_{eq}=EI\frac{(N+1)\alpha(N^2+2N+\alpha^2)}{(1-\alpha^2+\alpha^3)N^3+3\alpha N^2+(3+2\alpha-3\alpha^2+\alpha^3)\alpha^2N+\alpha^3} \quad (5)$$

Considering the perforated holes in the beam, the factor γ can be defined as a function of both the quantity of the holes along the section N and the fill factor represented by α as the following function:

$$\gamma=\frac{1}{6}\left(\frac{W}{L}\right)^2\gamma_F(N,\alpha) \quad (6)$$

Edelweiss Applied Science and Technology
ISSN: 2576-8484
Vol. 8, No. 6: 7404-7418, 2024
DOI: 10.55214/25768484.v8i6.3604

Where the variable $\gamma_F(N,\alpha)$ represents a suitable rational function based on its parameters:

$$\gamma_F = \frac{N(N^2+2N+\alpha^2)}{\alpha^2((\alpha^3-\alpha^2+1)N^3+3\alpha N^2+\alpha^2(\alpha^3-3\alpha^2+2\alpha+3)N+\alpha^3)} \quad (7)$$

The natural frequency of the perforated beam can be written as the expression used to compare in [26] as follows:

$$f_n = \frac{n\pi}{2L}\sqrt{\left(\frac{EI}{\rho_I}\right)\left(B_n - \sqrt{B_n^2 - \frac{\kappa G_A}{\pi^4 EI}\frac{\rho_I}{\rho_A}}\right)} \quad (8)$$

Where, B_n is defined by the formula as $B_n = \frac{1}{2\pi^2} + \frac{\kappa G_A}{2\pi^4 EI}\left(\frac{\rho_I}{\rho_A}\pi^2 + \frac{L^2}{n^2}\right)$, and κG_A is the shear rigidity with κ being the shear correction factor depending on the shape of the cross-section.

When using the assumption that cross-sections of the beam, which are perpendicular to its axis before it deforms, continue to stay flat and rotate to maintain their perpendicularity to the deformed axis, the natural frequencies of the Euler-Bernoulli beam can be presented using this formula [27]:

$$\omega_n^2 = \frac{\left(\frac{n\pi}{L}\right)^4\left(\frac{K_b}{I_0}\right)}{1+\left(\frac{I_1}{I_0}\right)\left(\frac{n\pi}{L}\right)^2} \quad (9)$$

With the Timoshenko beam, the expression determining natural frequency is as follows:

$$\omega_n^2 = \frac{\left(\frac{n\pi}{L}\right)^4\left(\frac{K_b}{I_0}\right)}{1+\left(\frac{K_b}{K_s}\right)\left(\frac{n\pi}{L}\right)^2} \quad (10)$$

In formulas (9) and (10), K_b and K_s denote the equivalent bending and shear stiffness of the perforated beam; $I_1 = \rho_{Ieq}$ and $I_0 = \rho_{Aeq}$ signify the equivalent rotational inertia and the equivalent mass per unit length, respectively.

Consider a referred solid beam with simply supported boundary condition and the following geometrical parameters: length $L = 4.352$ m; cross-sectional area $A = 1.31\times10^{-3}$ m^2; the area inertia moment $I = 5.71\times10^{-7}$ m^4; and the material properties: Modulus of elasticity $E = 202$ Gpa; modulus of rigidity $G = 77.7$ Gpa; mass density $\rho = 15267$ kg/m^3, and the shear correction factor $\kappa = 0.7$ [26], [27].

Table 2.
The first five natural frequencies of the solid beam (Hz).

Mode	[26]	[27]	Present study	
			FEM	ANSYS
1	6.3	6.296	6.2955	6.2934
2	25.18	25.136	25.1732	25.139
3	56.61	56.398	56.6229	56.432
4	100.52	99.873	100.676	100
5	156.85	155.281	157.4708	155.62

Edelweiss Applied Science and Technology
ISSN: 2576-8484
Vol. 8, No. 6: 7404-7418, 2024
DOI: 10.55214/25768484.v8i6.3604

In this section, we use finite-element-method (FEM) analysis in Matlab and simulation modal analysis in ANSYS to determine the first five natural frequencies of the referred beam. The results can be obtained in good agreement with the analytical results (see Table 2).

The results show that the first natural frequencies of the solid beam are the same with negligible error when using some different methods. This shows the convergence of the solution methods. To facilitate a comparative analysis of the frequency characteristics of a perforated single beam, a clamped-clamped beam with specific dimensions was selected. This beam, measuring 1401.1 µm, 46.9 µm, and 60 µm in length, width, and thickness, respectively, was chosen for its resemblance to the perforated beam in the referred research [28]. The body of the beam was then modified by introducing four lines of square holes, resulting in a total of 480 perforations. The material for the beams is selected as single crystal silicon with [1-0-0] orientation, E = 169 Gpa for Young's modulus, G = 79.6 Gpa for shear modulus, and ν = 0.064 for Poison's ratio. By using ANSYS software, the 3D model for this beam is built and the natural frequencies are analyzed. The finding results of this analysis with the fill factor α = 0.282 are presented in Table 3.

Table 3.
The first natural frequency of the mentioned perforated single beam (kHz).

Present study	[14]			Error %
	Model	Measured	FEM	
182.32	182.3	183.1	182.2	0.426

The results in Table 3 show a strong correlation between the simulated calculations from this study and the experimental results reported in [14], showing an error margin of just 0.426%. This result is also expressed in the previous research [28].

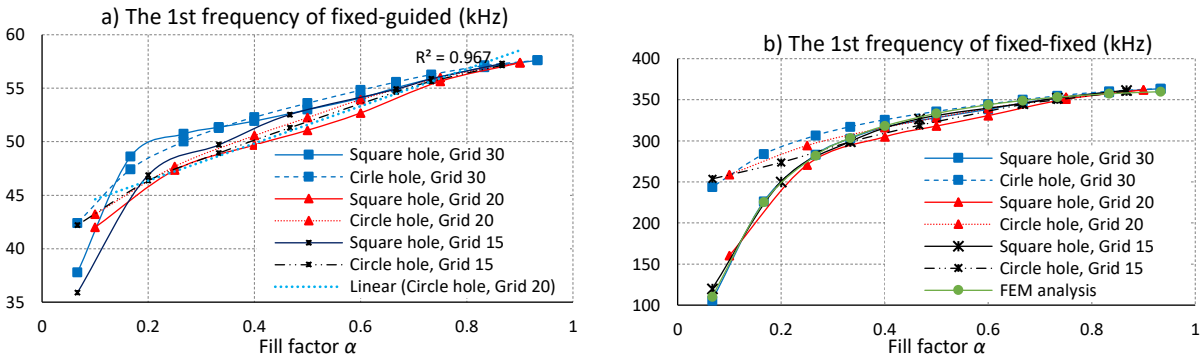

Figure 3.
The first frequency versus the fill factor.

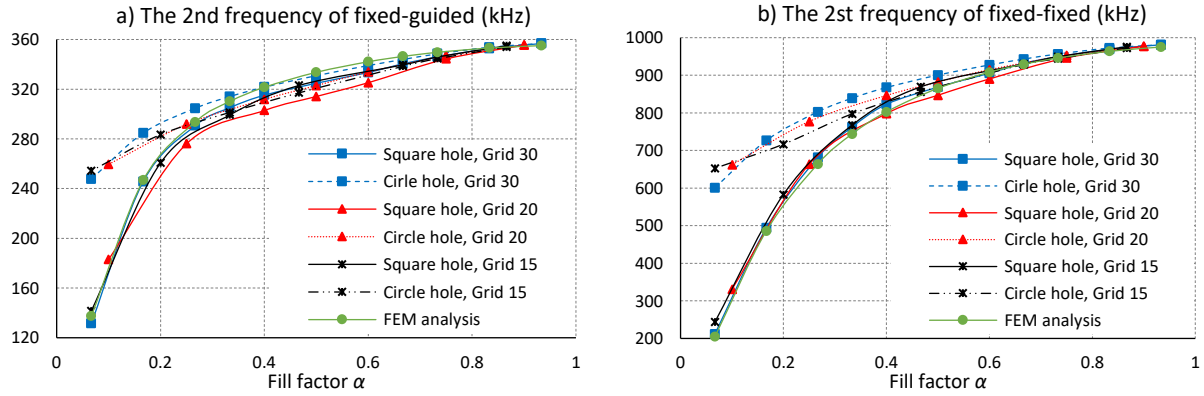

Figure 4.
The second frequency versus the fill factor.

Edelweiss Applied Science and Technology
ISSN: 2576-8484
Vol. 8, No. 6: 7404-7418, 2024
DOI: 10.55214/25768484.v8i6.3604

In the following section, the initial two fundamental frequencies of single beams with the aspect ratio L/h = 10 and the overall dimension of $L\times W\times h$ as 1200×120×60 micrometers will be assessed. This analysis will utilize the FEM and simulations conducted with ANSYS software under various boundary conditions. The holes are arranged into 2, 3, 4 rows and 40, 60, 80 columns for grid sizes 30, 20, and 15 μm, respectively in each case of the different grid size. The dimension of the holes (side on the square hole or diameter on the circle one) changes within the specified grid size. Consequently, following the expression (1), the fill factor α in this case is defined in the range from 0.067 to 0.93.

In Figure 3 and Figure 4, the first two major frequencies of the cutout holes single beam were presented with the two considered cases of the boundary condition: fixed-guided beam (one fixed end - one guided end) and fixed-fixed beam (2 fixed endings). The research was conducted with two forms for the cutout holes: square-shaped and circle-shaped. The increase in the fill factor α of the beam holes leads to a rise in the first two significant frequencies of a single beam. Consequently, as the size of the holes increases, the natural frequency experiences a decline. The most dramatic change in the frequencies was seen in the range $(0.05 - 0.4)$ of the fill factor α. As the size of the hole increases, the disparity becomes more pronounced. This difference is particularly evident with square holes. In the case of the circle-shaped cutout holes, the change in values of the first two frequencies is slower than those with square-shaped holes, and the relationship between the frequencies and fill factor is nearly linear with high R-square (R^2=0,967 in Figure 3a). When the fill factor α varies in the interval $0.4 \leq \alpha < 1$, the natural frequency values for both types of holes remain comparable, and the frequency changes appear to exhibit a linear trend. Varying boundary conditions result in distinct natural frequencies. For a fixed-fixed beam configuration, the first two frequencies are higher compared to a fixed-guided beam setup, with increases of 6.3 times for the first frequency and 2.7 times for the second one. The appearance of holes on the beam body alters the total mass and the area moment of inertia of the beams, consequently affecting the equivalent properties of the beams and altering the structural frequency.

3.2. The Equivalent and Natural Frequencies of Perforated Micro-Beam with Complex Structure

The stiffness of a beam is a critical component in the design of mechanical vibrational structures. Increased stiffness results in reduced deflection and allows for a higher operational frequency of the system. In most practical structures, the equivalent stiffness plays a direct role in determining the resonant frequency of resonators, such as microresonators. The calculation of this equivalent stiffness is performed through simulations that rely on the assumption about the the linearity in the mechanical response of the material. The conventional equation illustrates the relationship between deformation (δ) and stiffness (k) of a beam following Hooke's law as follows:

$$F = k \times \delta \tag{11}$$

This section will showcase the dynamic characteristics, such as equivalent stiffness - natural frequency, and resonant frequency - obtained through ANSYS Workbench for three typical microbeam types. In the Geometry module, the 3D models of these beams are detailed, featuring two types of holes present throughout each beam structure. The material properties can be found in Table 1 in the previous section.

3.2.1. Crab-Shaped Beam

A complex beam is formed by joining two single bars at right angles, resulting in an "L" or "Crab" shape and is called a Crab-shaped beam. Each bar is 200 and 300 μm length respectively with cross-section $W\times h$ = 16×30 μm. To calculate the equivalent stiffness of the beam, the displacement of the beam ending loaded with a unit force of 1 μN in the direction of vibration needs to be determined. The obtained deformation at the end of the beam is influenced by the properties of the material, geometric characteristics, and boundary conditions. Additionally, the dimensions and number of holes impact the equivalent stiffness. Figure 5 and Figure 6 illustrate the relation between the hole dimension and the dynamic characteristics of this beam with the holes arranged in one line in the plane of the beam. In the x-direction, the equivalent stiffness K_x changes slightly, ranging from 15 to 460 N/m as α varies from 0.065 to 0.875 respectively. In contrast, K_y experiences a broader

Edelweiss Applied Science and Technology
ISSN: 2576-8484
Vol. 8, No. 6: 7404-7418, 2024
DOI: 10.55214/25768484.v8i6.3604

variation, ranging from 22 to 1300 N/m with the same α values above featuring one end fixed and the other end guided in the crab beam setup (see Figure 5).

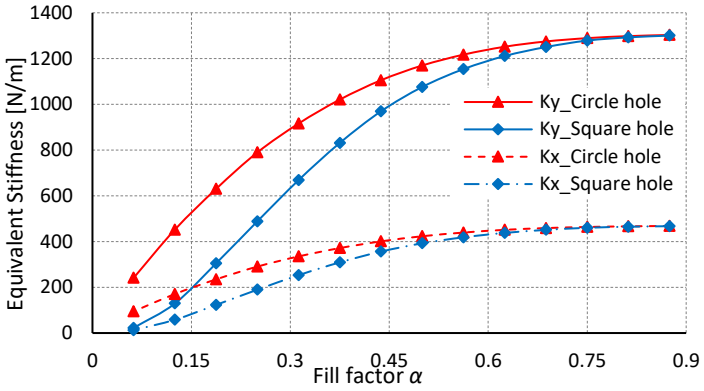

Figure 5.
The equivalent stiffness versus fill factor in the crab-shaped perforated beam.

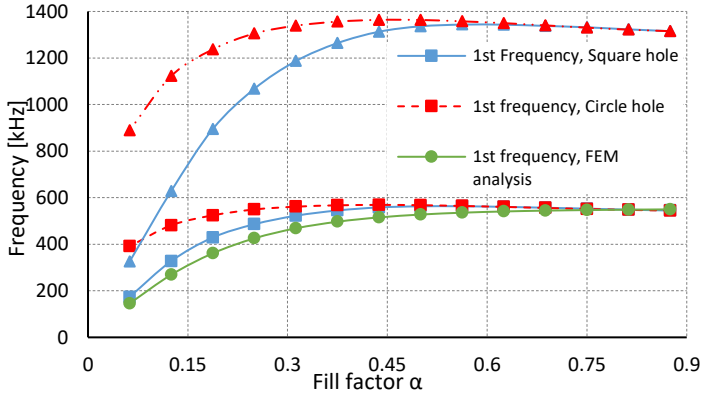

Figure 6.
Two first resonant frequencies of the perforated beam with crab-shaped.

Figure 6 illustrates the two initial frequencies, where the first one corresponds to the x-direction vibrational mode and the second one pertains to the y-direction vibrational mode of the beam. These are the desired modes of movement of the mechanical system in the MEMS devices. The distinction between these modes is minimal when the fill factor (α) is low ($\alpha < 0.2$), particularly in the case of square holes. As α approaches nearly 1 ($0.4 < \alpha < 0.875$), this difference increases and stabilizes. Additionally, Figure 6 depicts the comparison between the analytical calculations and simulations for the first frequency, showing a margin error of less than 10% for square holes. For square holes, both dynamic parameters exhibit lower values compared to those with circular holes. The findings indicate that the dynamic characteristics of the crab-shaped beam demonstrate limited variation as the fill factor approaches nearly 1, specifically for dimensions where d < 8 µm.

3.2.2. Folded Perforated Micro-Beam

The configuration of the micro folded beams consists of two or three or more single beams with $b \times h$ cross-section (Figure 2b). These single beams are connected thanks to the short bar with $b' \times h$ ($b' > b$) cross-section to restrict the unexpected mode of the whole beam. The geometrical parameters of this beam are 300 µm length, 16×30 µm cross-section for the main beam, and 40 µm, 35×30 µm respectively for the connecting bar.

Edelweiss Applied Science and Technology
ISSN: 2576-8484
Vol. 8, No. 6: 7404-7418, 2024
DOI: 10.55214/25768484.v8i6.3604

The relation between the equivalent stiffness of the folded perforated beam and the hole size (via the fill factor α) is nearly linear with R-square factors 0.9626 and 0.9712 for the circle and square shape of holes (Figure 7). The difference in value of these two results corresponding to two types of hole increases to raising of the hole size. The maximum deviation is up to 64% at $\alpha = 0.0625$ (corresponding to the size of hole d = 7.5 μm).

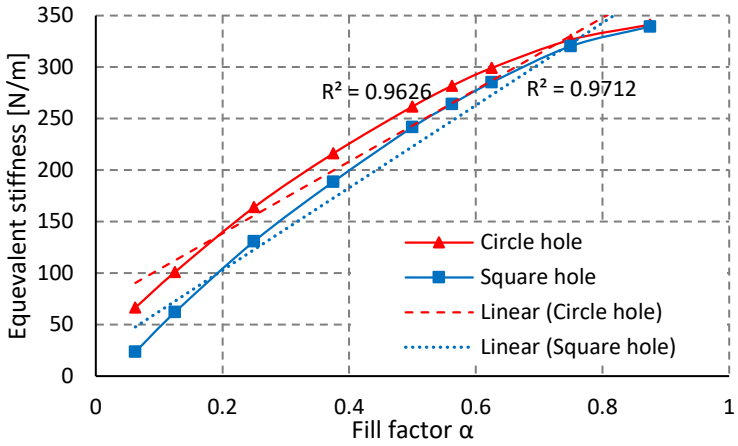

Figure 7.
Equivalent stiffness versus fill factor of the folded perforated beam.

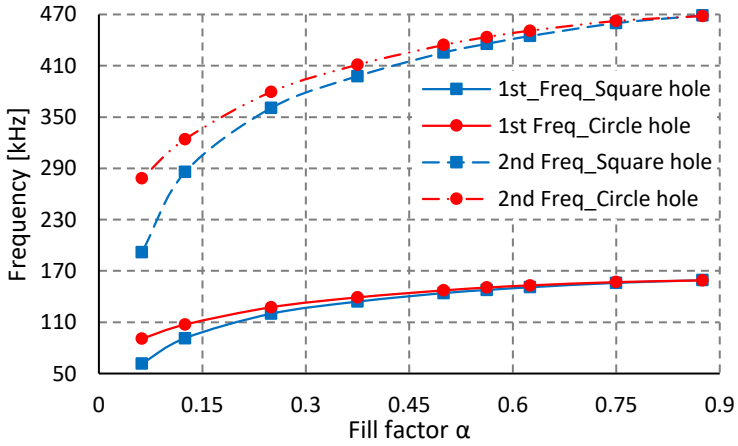

Figure 8.
The first two frequencies of the folded perforated beam.

Figure 8 presents the first two frequencies of the two principal modes in modal analysis for the considered folded perforated beam. The received results show that the frequency deviation between these two major frequencies is 130 up to 310 kHz and guarantees to restrict the unexpected modes in operating the MEMS devices in which this folded beam is used. The first one of them in both types of holes varies more lightly than the second one in a range from 61 to 159 kHz. Although the increase in the size of the hole causes the decrease of the both two main frequencies, the frequency deviation tends to increase from 195% up to 213%. As the hole size increases, the frequency values of the two principal modes decrease, in which the two frequencies of the beam with square holes decrease faster than those of circle holes.

3.2.3. V-Shaped Perforated Beam

Edelweiss Applied Science and Technology
ISSN: 2576-8484
Vol. 8, No. 6: 7404-7418, 2024
DOI: 10.55214/25768484.v8i6.3604

The configuration of the V-shaped beam is nearly similar to the folded beam without a connecting bar and two bars forming a small angle. The geometrical parameters for this beam are 250 µm length and 16×30 µm cross-section.

The equivalent stiffness and the first two frequencies of two major modes of the V-shaped perforated beam are shown in Figure 9 and Figure 10, respectively. The variability of the two frequencies with two types of holes cut out is different. Similar to the previous beams, when the holes are cut into the circle, the first frequency varies in a small range (286-386 kHz) corresponding to the fill factor α from 0.1 to 0.875 (the diameter hole from 2 to 14.5 µm). The difference in the second frequency is stronger than in both types of holes. The frequency deviation with minimum and maximum hole size is 946 kHz (57%) and 635 kHz (38%) in square holes and circle holes respectively. Similarly, the equivalent of the V-shaped beam also variates more smoothly to the fill factor in the case of the circle-perforated holes. The findings indicate that the dynamic characteristics of beams containing circular holes exhibit a smoother variation compared to those featuring square holes. This can be explained that the cross-section area of the beam with circle holes changes more slowly than that with square holes.

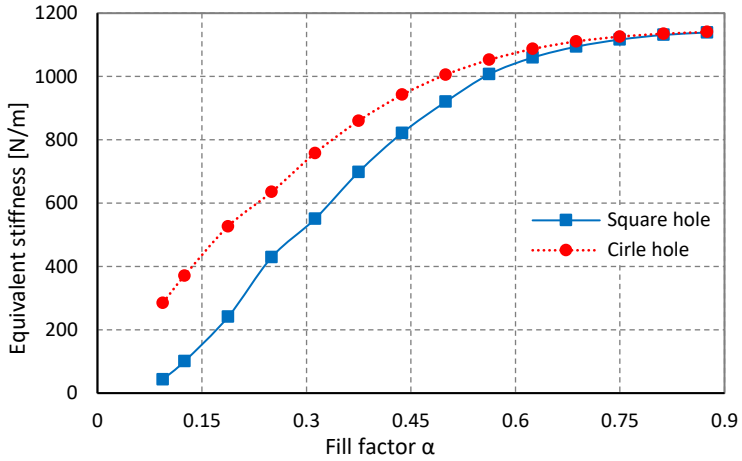

Figure 9.
Equivalent stiffness versus fill factor of V-shaped perforated beam.

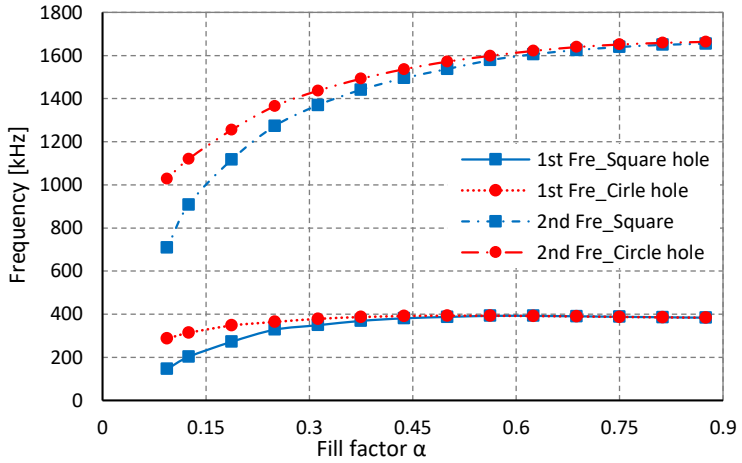

Figure 10.
The first two frequencies of the V-shaped perforated beam.

3.3. Air Damping with Perforated Beams

Edelweiss Applied Science and Technology
ISSN: 2576-8484
Vol. 8, No. 6: 7404-7418, 2024
DOI: 10.55214/25768484.v8i6.3604

Air damping is associated with the surface area of the moving components in the MEMS devices. This phenomenon plays a crucial role in evaluating the dynamic performance of micromechanical devices and systems, particularly because of the significant surface area-to-volume ratio of their moving components. In the vibration micromechanical system, such as in a beam–mass system (with k, m, c), the coefficient of damping force is an important dynamic parameter. It appears in the expressions that determine the damping ratio ζ and the quality factor Q used to characterize the mechanical system.

$$\zeta = \frac{c}{2\sqrt{mk}};\ Q = \frac{1}{2\zeta} = \frac{\sqrt{mk}}{c} \tag{12}$$

Air damping has two primary elements: slide air damping and squeeze air damping. Squeeze film damping occurs when two parallel plates move orthogonally to each other. The pressure differential in the fluid around the moving microdevices produces damping forces. Slide film damping occurs when two parallel plates move tangentially in relation to one another. In this configuration, the motion of the movable component is limited to a sliding movement parallel to the substrate. Consequently, the damping coefficient for this beam model is solely attributed to sliding damping. Two principal damping models often used in slide damping analysis are the Couette-type model and the Stokes-type model. The Couette-type model is relevant when the gap between the moving element and the stationary substrate is low; otherwise, the Stokes-type model is more appropriate for analyzing slide film damping.

For the case of slide air damping: given that the gap distance (distance from mass to substrate), denoted as h, is significantly smaller than δ – the effective decay distance $\delta = \sqrt{2\mu/\rho\omega}$ (the distance from the top of the moving part to the cover of the device), and only considering the damping on the bottom of the beam, the damping coefficient takes the form of a Couette-flow type and can be represented as [29], [30]:

$$c = \mu \frac{A_d}{h} \tag{13}$$

Where A_d is the effective surface area of the beams (this area is the rest of the surface of the beam after perforating the holes); $\mu = 1.7984\times10^{-6}$ (Ns/m^2) is the viscosity of air.
Taking into account the holes on the face of the beam, the effective area A_d can be calculated by:

$$A_d = A_t - A_h \tag{14}$$

For each case of beams mentioned above, the total area A_t and the hole area A_h are determined and shown in Table 4, here, 31, 120, and 28 are the number of the holes on the face beam of crab-beam, folded beam, and V-shaped beam, respectively.

Table 4.
The surface area of the mentioned different beams.

		Crab-beam	Folded-beam	V-shaped beam
Total area A_t (μm^2)		8256	9600	7600
Hole area A_h (μm^2)	Square hole	$31\times w^2$	$120\times w^2$	$28\times w^2$
	Circle hole	$31\times\pi\times d^2/4$	$120\times\pi\times d^2/4$	$28\times\pi\times d^2/4$

Given the gap distance h = 6 μm for the common case, and using the expressions (13) and (14), the damping coefficient versus fill factor is determined and shown in Figure 11.

The results in Figure 11 show that the damping coefficient in the beams with circle holes cutout is higher than the beam with square holes for all of the above types of microbeams. This phenomenon can be explained as the beam with the same hole dimension but the area of a circle hole is smaller than a square hole, therefore the effective area of the beam with circle holes is larger than the beam with square holes with the same number and distribution of the holes. This leads to an increase in the damping force to the beam with circle holes. The damping coefficient reaches the minimum value of 0.0625 at the largest hole size. It is significantly reduced compared to the full-fill beam at this value of fill factor (70%, 84%, 77% reduction in case of square holes and 55%, 66%, 60% reduction in case of circle holes for folded, crab and

Edelweiss Applied Science and Technology
ISSN: 2576-8484
Vol. 8, No. 6: 7404-7418, 2024
DOI: 10.55214/25768484.v8i6.3604

V-shaped beam, respectively). These values are ideal and will not be achieved in practice. Commonly, the value of the fill factor needs to be set at 0.2 - 0.8 to guarantee convenience in the fabrication. At the value of 0.25, the reduction compared with the full fill beam is 44%, 53%, 52% with square holes, and 35%, 42%, and 41% with circle holes for the folded, crab, and V shape beam, respectively (Figure 12).

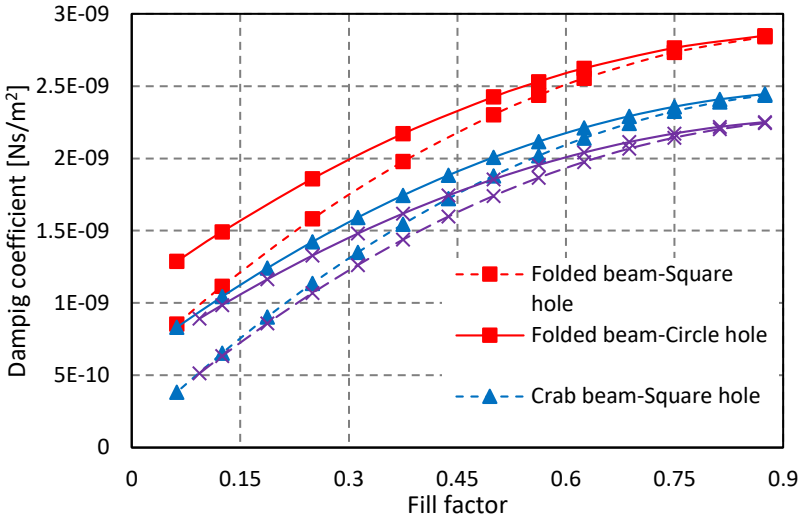

Figure 11.
Damping coefficient versus fill factor.

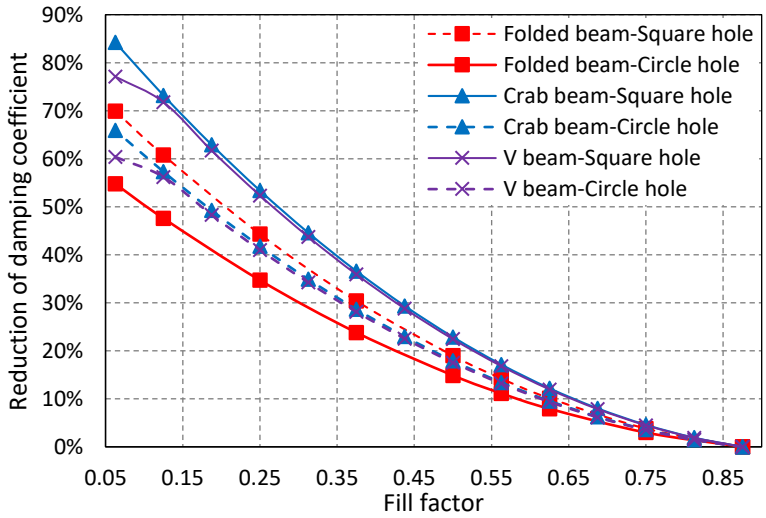

Figure 12.
The reduction of damping coefficient versus fill factor.

4. Conclusion

The paper presented three perforated beam models with complex structures, consisting of the folded, crab, and V-shaped beam. The dynamic characteristics of these beams such as the equivalent stiffness, the major frequencies, and the damping coefficient were determined by using analytical and simulation analysis using ANSYS software. Besides, the obtained results for the single beam in this study also were compared with the previous research with a 0.426% error. The results again confirm the influence of the holes cut out of the elastic beam on their dynamic characteristics. The existence of perforated holes leads to a reduction in the equivalent stiffness of beams, which subsequently lowers the working frequencies of

Edelweiss Applied Science and Technology
ISSN: 2576-8484
Vol. 8, No. 6: 7404-7418, 2024
DOI: 10.55214/25768484.v8i6.3604

the system. In addition, the holes in the beam body also cause the reduction of the damping force of the air in the operating environment thanks to the decrease in damping coefficient. The maximum decrease in damping coefficient reaches 84% in the ideal case for the crab beam with square holes. The hole size needs to be chosen to guarantee the value of the fill factor is in the range of 0.2-0.8 for convenience in the fabrication process. Finally, the shape of the perforated holes also affects the variable of the dynamic response of the beams, where the circle hole causes change less than the square hole.

Acknowledgments:
This research is funded by the Le Quy Don Technical University Research Fund under code 23.01.16.

References

[1] J. L. Barth and M. A. G. Darrin, "Systems engineering for microscale and nanoscale technologies," *Syst. Eng. Microscale Nanoscale Technol.*, pp. 1–549, 2016, doi: 10.1201/b11291-3.
[2] S. F. Krar and A. Gill, "Exploring Advanced Manufacturing Technologies," p. 448, 2003.
[3] J. W. Judy, "Microelectromechanical systems (MEMS): Fabrication, design and applications," *Smart Mater. Struct.*, vol. 10, no. 6, pp. 1115–1134, 2001, doi: 10.1088/0964-1726/10/6/301.
[4] Y. Shen, "Current Status and Application of Micro-electromechanical Systems (MEMS)," *Highlights Sci. Eng. Technol.*, vol. 46, pp. 97–105, 2023, doi: 10.54097/hset.v46i.7685.
[5] D. Van Hieu, L. Van Tam, N. Van Duong, N. Duy Vy, and C. M. Hoang, "Design and Simulation Analysis of A Z Axis Microactuator with Low Mode Cross-Talk," *J. Mech.*, vol. 36, no. 6, pp. 881–888, 2020, doi: 10.1017/jmech.2020.48.
[6] H. Din, F. Iqbal, and B. Lee, "Modelling and optimization of single drive 3-axis MEMS gyroscope," *Microsyst. Technol.*, vol. 26, no. 9, pp. 2869–2877, 2020, doi: 10.1007/s00542-020-04840-7.
[7] V. T. Vu and D. T. Chu, "Determine the dynamic parameters in mechanical system of the crab-shaped MEMS vibratory gyroscope," *Microsyst. Technol.*, vol. 27, no. 9, pp. 3429–3435, 2021, doi: 10.1007/s00542-020-05128-6.
[8] S. E. Alper and T. Akin, "Symmetrical and decoupled nickel microgyroscope on insulating substrate," *Sensors Actuators, A Phys.*, vol. 115, no. 2-3 SPEC. ISS., pp. 336–350, 2004, doi: 10.1016/j.sna.2004.04.041.
[9] K. T. Hoang, D. T. Nguyen, and P. H. Pham, "Impact of design parameters on working stability of the electrothermal V-shaped actuator," *Microsyst. Technol.*, vol. 26, no. 5, pp. 1479–1487, 2020, doi: 10.1007/s00542-019-04682-y.
[10] K. Guha, H. Dutta, J. Sateesh, S. Baishya, and K. Srinivasa Rao, "Design and analysis of perforated MEMS resonator," *Microsyst. Technol.*, vol. 27, no. 2, pp. 613–617, 2021, doi: 10.1007/s00542-018-4207-5.
[11] K. Guha, N. M. Laskar, H. J. Gogoi, K. L. Baishnab, and K. S. Rao, "A new analytical model for switching time of a perforated MEMS switch," *Microsyst. Technol.*, vol. 26, no. 10, pp. 3143–3152, 2020, doi: 10.1007/s00542-018-3803-8.
[12] M. A. Alazwari, A. A. Abdelrahman, A. Wagih, M. A. Eltaher, and H. E. Abd-El-Mottaleb, "Static analysis of cutout microstructures incorporating the microstructure and surface effects," *Steel Compos. Struct.*, vol. 38, no. 5, pp. 583–597, 2021, doi: 10.12989/scs.2021.38.5.583.
[13] K. Guha *et al.*, "An improved analytical model for static pull-in voltage of a flexured MEMS switch," *Microsyst. Technol.*, vol. 26, no. 10, pp. 3213–3227, 2020, doi: 10.1007/s00542-018-3911-5.
[14] L. Luschi and F. Pieri, "An analytical model for the determination of resonance frequencies of perforated beams," *J. Micromechanics Microengineering*, vol. 24, no. 5, 2014, doi: 10.1088/0960-1317/24/5/055004.
[15] A. A. Abdelrahman and M. A. Eltaher, "On bending and buckling responses of perforated nanobeams including surface energy for different beams theories," *Eng. Comput.*, vol. 38, no. 3, pp. 2385–2411, 2022, doi: 10.1007/s00366-020-01211-8.
[16] I. Esen, A. A. Abdelrahman, and M. A. Eltaher, "Dynamics analysis of timoshenko perforated microbeams under moving loads," *Eng. Comput.*, vol. 38, no. 3, pp. 2413–2429, 2022, doi: 10.1007/s00366-020-01212-7.
[17] W. N. Sharpe, R. Vaidyanathan, B. Yuan, G. Bao, and R. L. Edwards, "Effect of etch holes on the mechanical properties of polysilicon," *J. Vac. Sci. Technol. B Microelectron. Nanom. Struct. Process. Meas. Phenom.*, vol. 15, no. 5, pp. 1599–1603, 1997, doi: 10.1116/1.589554.
[18] V. L. Rabinovich, R. K. Gupta, and S. D. Senturia, "Effect of release-etch holes on the electromechanical behavior of MEMs structures," *Int. Conf. Solid-State Sensors Actuators, Proc.*, vol. 2, pp. 1125–1128, 1997, doi: 10.1109/sensor.1997.635400.
[19] S. S. Mohite, H. Kesari, V. R. Sonti, and R. Pratap, "Analytical solutions for the stiffness and damping coefficients of squeeze films in MEMS devices with perforated back plates," *J. Micromechanics Microengineering*, vol. 15, no. 11, pp. 2083–2092, 2005, doi: 10.1088/0960-1317/15/11/013.
[20] W. H. Tu, W. C. Chu, C. K. Lee, P. Z. Chang, and Y. C. Hu, "Effects of etching holes on complementary metal oxide semiconductor- microelectromechanical systems capacitive structure," *J. Intell. Mater. Syst. Struct.*, vol. 24, no. 3, pp. 310–317, 2013, doi: 10.1177/1045389X12449917.

[21] N. Van Dung, L. M. Thai, N. T. Dung, and P. Van Minh, "Free Vibration Response of Micro FG Beams Taking the Initial Geometrical Imperfection into Consideration," *Lect. Notes Mech. Eng.*, pp. 197–203, 2023, doi: 10.1007/978-3-031-31824-5_24.
[22] "On the free vibration analysis of micro FG beams considering the initial geometrical imperfection".
[23] T. C. N. Nguyen, "Static Bending Analysis of Variable Thickness Microplates Using the Finite Element Method and Modified Couple Stress Theory," *J. Sci. Tech.*, vol. 17, no. 3, 2022, doi: 10.56651/lqdtu.jst.v17.n03.351.
[24] T. Ozaki, N. Ohta, and M. Fujiyoshi, "Analytical modeling of a MEMS beam resonator with release-etch holes," *J. Micromechanics Microengineering*, vol. 32, no. 9, 2022, doi: 10.1088/1361-6439/ac809a.
[25] H. BENAROYA, T. Wei, and S. HAN, "Dynamics of Transversely Vibrating Beams Using Four Engineering Theories," *J. Sound Vib.*, vol. 225, no. 5, pp. 935–988, 1999.
[26] Y. Song, T. Kim, and U. Lee, "Vibration of a beam subjected to a moving force: Frequency-domain spectral element modeling and analysis," *Int. J. Mech. Sci.*, vol. 113, pp. 162–174, 2016, doi: 10.1016/j.ijmecsci.2016.04.020.
[27] A. A. Abdelrahman, M. A. Eltaher, A. M. Kabeel, A. M. Abdraboh, and A. A. Hendi, "Free and forced analysis of perforated beams," *Steel Compos. Struct.*, vol. 31, no. 5, pp. 489–502, 2019, doi: 10.12989/scs.2019.31.5.489.
[28] V. Van The, "Dynamic response of the micro-perforated crab beam used in MEMS vibratory gyroscope device," *Vietnam J. Mech.*, 2024, doi: 10.15625/0866-7136/19477.
[29] P. Effect and R. Tensor, "Analysis and Design Principles of MEMS Devices-第六章," 1954.
[30] W. Wang, J. Jia, and J. Li, "Slide film damping in microelectromechanical system devices," *Proc. Inst. Mech. Eng. Part N J. Nanoeng. Nanosyst.*, vol. 227, no. 4, pp. 162–170, 2013, doi: 10.1177/1740349913486097.
[31] D. V. Quang, N. D. Tran, D. T. Luat, T. V. Do, "Static analysis and boundary effect of FG-CNTRC cylindrical shells with various boundary conditions using quasi-3D shear and normal deformations theory," *Struct.*, vol. 44, pp. 828–850, 2022, doi: 10.1016/j.istruc.2022.08.039.
[32] P. V. Vinh, N. T. Dung, N. C. Tho, T. V. Do, N. T. Trung, L. K. Hoa, "Modified single variable shear deformation plate theory for free vibration analysis of rectangular FGM plates," *Strut.*, vol. 29, pp. 1435-1444, 2021, doi: 10.1016/j.istruc.2020.12.027.
[33] D. H. Duc, T. V. Do, P. M. Phuc, "Buckling Analysis of Variable Thickness Cracked Nanoplatesconsiderting the Flexoelectric Effect," *Trans. Comm. Scie. J.*, vol. 73, no. 5, pp. 470-485, 2022, doi: 10.47869/tcsj.73.5.3
[34] N.C. Tho, N.T. Ta, T. V. Do, "New numerical results from simulations of beams and space frame systems with a tuned mass damper," *Materials*, vol. 12, no. 8, 1329, 2019, doi: 10.3390/ma12081329
[35] D. M. Tien, T. V. Do, N.T.H. Van, A. Tounsi, P.V. Minh, D.N. Mai, "Buckling and forced oscillation of organic nanoplates taking the structural drag coefficient into account," *Comp. Concr.*, vol. 6, no. 32, pp. 553-565, 2024, doi:10.12989/cac.2023.32.6.553

Edelweiss Applied Science and Technology
ISSN: 2576-8484
Vol. 8, No. 6: 7404-7418, 2024
DOI: 10.55214/25768484.v8i6.3604